Article

A fluorescent Hsp90 probe demonstrates the unique association between extracellular Hsp90 and malignancy in vivo

Lauren B Crowe, Philip F Hughes, David A Alcorta, Takuya Osada, Aaron P Smith, Juliane Totzke, David R. Loiselle, Isaac D Lutz, Madhusudhana Gargesha, Debasish Roy, Jose Roques, David Darr, H. Kim Lyerly, Neil L Spector, and Timothy AJ Haystead

Just Accepted

A fluorescent Hsp90 probe demonstrates the unique association between extracellular Hsp90 and malignancy *in vivo*

Authors: Lauren B Crowe[1,‡]; Philip F Hughes[2,‡]; David A Alcorta[3]; Takuya Osada[4]; Aaron P Smith[2]; Juliane Totzke[2]; David R Loiselle[2]; Isaac D Lutz[2]; Madhusudhana Gargesha[5]; Debasish Roy[5]; Jose Roques[6]; David Darr[6]; H Kim Lyerly[4]; Neil L Spector[2]; Timothy AJ Haystead[2*]

[1]Department of Cell Biology, Duke University, Durham, NC 27710 USA

[2]Department of Pharmacology and Cancer Biology, Duke University, Durham, NC 27710 USA

[3]Department of Medicine, Duke University, Durham, NC 27710 USA

[4]Department of Surgery, Duke University, Durham, NC 27710 USA

[5]BioInVision, Inc., Mayfield Village, OH 44143 USA

[6]Lineberger Comprehensive Cancer Center, University of North Carolina, Chapel Hill, NC 27599 USA

[*]Corresponding author, Timothy Haystead, Email: timothy.haystead@dm.duke.edu, tel: (919) 613-8606

[‡]These authors contributed equally to this work.

1
2
3
4
5
6
7
8
9
10
11
12
13
14
15
16
17
18
19
20
21
22
23
24
25
26
27
28
29
30
31
32
33
34
35
36
37
38
39
40
41
42
43
44
45
46
47
48
49
50
51
52
53
54
55
56
57
58
59
60

Abstract

Extracellular expression of heat shock protein 90 (eHsp90) by tumor cells is correlated with malignancy. Development of small molecule probes that can detect eHsp90 *in vivo* may therefore have utility in the early detection of malignancy. We synthesized a cell impermeable far-red fluorophore-tagged Hsp90 inhibitor to target eHsp90 *in vivo*. High resolution confocal and lattice light sheet microscopy show that probe-bound eHsp90 accumulates in punctate structures on the plasma membrane of breast tumor cells and is actively internalized. The extent of internalization correlates with tumor cell aggressiveness, and this process can be induced in benign cells by over-expressing p110HER2. Whole body cryoslicing, imaging and histology of flank and spontaneous tumor-bearing mice strongly suggests that eHsp90 expression and internalization is a phenomenon unique to tumor cells *in vivo* and may provide an 'Achilles heel' for the early diagnosis of metastatic disease and targeted drug delivery.

Heat shock protein 90 (Hsp90) comprises 1—3% of the cellular protein and acts as a molecular chaperone for over 200 client proteins [1,2]. Many cancer cells upregulate Hsp90 expression and are believed to be "addicted" to the protein to maintain proper folding of overexpressed oncoproteins [3]. Thus, 17 distinct Hsp90 inhibitors have entered clinical trials as potential cancer treatments [4]. These inhibitors bind to the ATP-binding pocket of Hsp90 and its paralogs GRP94 and TRAP1, inhibiting chaperone function [5]. In tumor cells, inhibiting Hsp90 results in the degradation of oncogenic client proteins and arrest of cell growth. When administered as a monotherapy in clinical studies, Hsp90 inhibitors tend to promote tumor growth arrest rather than regression [4], which is generally thought to be related to a compensatory induction of Hsp70. However, if drug surveillance is maintained, responsive patients remain in stable disease [6].

The great conundrum of Hsp90 therapy is the molecular mechanism by which Hsp90 inhibitors exhibit any therapeutic efficacy given its abundance and ubiquitous expression *in vivo*. Genetic deletion studies have shown that Hsp90 is essential for normal cell function [3]; yet, systemic inhibition of Hsp90 is well tolerated in humans, with dose-limiting toxicities characterized by diarrhea and a reversible night blindness with some Hsp90 inhibitors [7]. The biodistribution of radio-labeled PUH71, a cell permeable Hsp90 inhibitor, has been studied in mice bearing MDA-MB-468 xenografts [8,9]. Consistent with the broad expression of Hsp90, radioactivity was initially detected in all tissues. However, 24 hours after injection, the tumor became visible due to clearance of the drug from normal tissues and drug retention in the tumor. An earlier study hypothesized that Hsp90 in cancer cells is in a more active conformation by existing in a complex with several co-chaperones. Hsp90 in this "active" conformation has a

Page **3** of **26**

higher affinity for ATP and Hsp90 inhibitors and is thus more susceptible to inhibition [10]. In addition, Hsp90 phosphorylation by the mitotic checkpoint kinase Mps1 results in increased Hsp90 client association and sensitivity to cell-permeable Hsp90 inhibitors, such as SNX2112 and Ganetespib, in renal cancer cells [11-13].

Of interest to us is an extracellular Hsp90 (eHsp90) and its association with malignant behavior [14, 15]. In tumor cells, eHsp90 is thought to chaperone external proteins responsible for migration and metastasis, such as matrix metalloproteinases. Previous work by our group with fluorophore-tethered Hsp90 inhibitors also confirmed trafficking of Hsp90 to the cell surface but also showed that the protein was reinternalized [16]. Two groups have also demonstrated reinternalization of eHsp90 in dendritic antigen presenting cells and hypothesize that it is required for antigen cross presentation, and its reinternalization is a dynamin-independent Cdc42-dependent process [12, 17]. Together, these studies suggest that expression of eHsp90 and reinternalization has specific functions *in vivo*.

To explore eHsp90 expression *in vivo*, we developed the eHsp90 inhibitor HS-131 and its inactive analog HS-198. We show that these far-red dye-tethered Hsp90 inhibitors can be reproducibly synthesized and fluoresce at wavelengths that have low natural background fluorescence. Microscopic analysis shows that probe binding promotes eHsp90 aggregation followed by internalization in more aggressive tumor cells. Furthermore, overexpression of oncogenic p110HER2 in benign cells stimulates eHsp90 trafficking, aggregation, and reinternalization, suggesting that cycling of the protein is part of a larger oncogenic process associated with malignancy. Lastly, full microscopic analysis of mice bearing either flank or

spontaneous mammary tumors underscores the uniqueness of eHsp90 expression and

internalization in tumor cells.

RESULTS AND DISCUSSION

Synthesis and characterization of HS-131. Previously, we reported on the synthesis and

characterization of tethered Hsp90 inhibitors, HS-69 and HS-27, consisting of a modified Hsp90

inhibitor tethered to a near infrared (nIR) probe and FITC, respectively [16]. However, HS-27 was

not optimized for higher resolution confocal imaging or tissue penetration, and HS-69 was

tethered to an expensive and proprietary nIR dye of partially unknown structure via a potentially

labile amide linker. We thus decided to synthesize a new Hsp90 inhibitor, HS-131, tethered to a

Cy5 dye that was more stable and reproducibly synthesized (Fig. 1a). A far-red probe with peak

wavelengths of excitation and emission at 646 and 665 nm, respectively (Fig. S1a), was chosen

over a nIR dye to maintain imaging compatibility. On HS-198, a critical primary amide required

for inhibitor binding in the active site of Hsp90 is replaced with a dimethyl amide group that

precludes the formation of a critical hydrogen bond within the ATP-binding pocket of Hsp90 [18].

The complete synthesis of HS-131 and HS-198 is shown in Fig. 1b. The tethered Hsp90

ligand **5**, HS-23 [19], was converted by reductive amination to the boronic acid **6**. An amine

linkage was chosen to avoid hydrolytic liabilities *in vivo*. Suzuki coupling [20] with dye **8** [21]

produced HS-131. HS-198 was prepared in analogous fashion from amine **13**. Amine **13** was

prepared from amine **5** as shown in Fig. 1c. Amine **5** was first protected as the BOC amide **11**.

The primary amide was then alkylated by treating **11** with sodium t-butoxide in THF followed by

slow addition of methyl iodide. Chromatography gave the clean dimethyl amide **12** with 45%

yield. Analysis of the ^{1}H-NMR and COSY spectra of **12** showed the addition of two methyl groups, loss of the primary amide protons, and retention of the aniline and BOC amide protons. Deprotection with TFA afforded the desired amine **13**, which was converted as described above to HS-198 (Fig. 1c). Complete synthesis details are listed in the supplementary methods.

In a thermal stability assay [16, 19], HS-131 but not HS-198 stabilized purified Hsp90 (Fig. S1b, c). In addition, HS-23, which mimics the structure of HS-131 without the fluorophore, showed specificity to Hsp90 over Grp94 at higher concentrations, unlike previously published inhibitor HS-10 (Fig. S1d). Furthermore, HS-131 specifically eluted Hsp90 from lysates applied to an ATP resin, whereas HS-10 and Ganetespib eluted Hsp90 and Grp94 (Fig. S1e). HS-198 did not elute Hsp90 except at high concentrations. None of the tested drugs eluted TRAP1 from the ATP resin. Studies with HS-152 (Fig. S2b), containing the Cy5 fluorophore and PEG linker but lacking the Hsp90 ligand, showed no affinity for Hsp90 in thermal stability or in ATP competition studies, ruling out any contribution of the fluorophore moiety to protein binding (Fig. S1b-c, S3a-b). These studies support the specificity of HS-131 for Hsp90.

HS-131 visualizes tumor cell-specific eHsp90. HS-131 is not cell permeable and binds exclusively to eHsp90, allowing us specific access to this particular pool of one of the most abundant proteins in the cell. To analyze the internalization of eHsp90 in transformed cells, we utilized the 4T1 cell model. The five isogenic cell lines (67NR, 168FARN, 4T07, and 4T1) are isolated from a single spontaneous mammary tumor and exhibit varying degrees of metastatic disease when injected into mice [22]. HS-131 was internalized more in 4T1 cells (the most aggressive of the five lines) over the less metastatic lines (Figs. 2a, b). In MDA-MB-468 cells,

uptake of HS-131 was dose- and time-dependent (Fig. 2c, d), and binding of the probe to eHsp90 was competed with HS-10 and PUH71 (Fig. 2e). In contrast, the inactive analog HS-198 was only weakly internalized at higher concentrations (Fig. 2c).

Hsp90 internalization is inhibitor-independent. To determine if eHsp90 internalization is dependent on Hsp90 inhibition by HS-131 or is a natural oncogenic mechanism, we employed a biotin internalization assay [23]. Cells were treated on ice with amine-reactive biotin to label extracellular proteins. The cells were returned to 37°C to allow for endocytosis, cooled again, and stripped of any extracellular biotin. By Western blot of avidin-purified lysates, we observed the presence of biotin-labeled Hsp90 in the cell lysates after internalization, suggesting that the external eHsp90 had been biotinylated and actively reinternalized (Fig. 2f).

HS-131 binding reveals eHsp90 puncta. Confocal images of HS-131-treated cells revealed striking punctate formations both on the cell surface and within the cell itself, as well as diffuse fluorescence throughout the cell (Fig. 3a, Movie S1). Close examination of the larger structures shows that the average size of these puncta is 0.95 ± 0.04 μm^3 with an average fluorescence intensity of 33.01 ± 10.37 units. Using a standard fluorescence curve (Fig. S3f), we estimated the concentration within the puncta of HS-131 to be 4.66 ± 0.05 μM. Based on puncta volume and a ratio of 1:1 for HS-131:Hsp90 monomer, we estimate that the larger puncta contain 2659 ± 105 monomers of eHsp90. Accumulation of the puncta intracellularly is time-dependent (Fig 3b).

We demonstrated that formation of the puncta is eHsp90-dependent in multiple ways; first, HS-152, the tethered fluorophore without the ligand, does not form puncta when applied to cells (Figs. S3a-c); second, HS-27, a FITC-tethered Hsp90 inhibitor with a fluorophore moiety

Page **7** of **26**

structurally unrelated to the Cy5 based fluorophore used in HS-131, forms puncta when applied

to tumor cells (Fig. S3d); thirdly, binding of HS-131 and HS-27 to eHsp90 is blocked by

structurally distinct Hsp90 inhibitors, such as PUH71 (Fig. 2e); fourth, puncta do not form on

non-malignant cells in the presence of HS-131 or HS-27 (Fig. 2a, [16]). Additionally, formation of

the puncta is reversible within cells; internal puncta number decrease after drug removal, and

diffuse fluorescence can be observed throughout the cell (Fig. 3a). This diffusion may be a result

of exchange with intracellular ATP or the degradation of the internalized eHsp90. Probe

aggregates would not be expected to spontaneously dissipate without the addition of an organic

solvent.

Live imaging of HS-131-treated cells reveals active trafficking of puncta (Movie S2),

suggesting that their formation is part of an organized biological process. Live imaging was also

performed on cells treated with HS-131 alone, HS-198, or HS-131 and HS-10, and spots were

tracked over time to investigate any differences in puncta movement and size. HS-131-treated

cells exhibited significantly more puncta; however, puncta size and speed of movement did not

appear to be affected with various treatments (Fig. 3d, Fig. S3g-h). HS-131 puncta were

competed with HS-10 (Fig. 3d). No puncta were observed to travel to or within the nucleus. The

puncta are therefore a natural phenomenon occurring in live malignant cells only that have been

revealed by the HS-131 probe. HS-131 is much smaller than antibodies compared with Hsp90

(Fig. S2a); thus, HS-131 is more suited for unobtrusive labeling of eHsp90 puncta. However,

colocalization of HS-131 with eHsp90 was confirmed using antibodies (Fig. 3c).

Hsp90 is known to undergo conformational changes as it cycles between its ATP- and ADP-bound state, altering its affinity for its clients and co-chaperones [24-26]. Biochemical studies using affinity resins to isolate the extracellular pool strongly support this hypothesis; eHsp90 was consistently recovered in highly purified form in the absence of clients, co-chaperones or modifications. Therefore, the probe-bound state may be akin to a locked conformation induced upon drug binding, permanently releasing its clients and co-chaperones at the plasma membrane. It is plausible that in this 'spent' state, the protein self-aggregates on the membrane to form puncta, and this signals its reinternalization.

eHsp90 is actively internalized. To determine the potential mechanism of eHsp90 re-internalization, we adopted an unbiased approach by investigating the impact of several small molecule inhibitors known to selectively interfere with various mechanisms of protein trafficking in and out of cells. Of the 5 inhibitors tested, only cytochalasin D (CytoD, actin inhibitor) inhibited HS-131 uptake (Fig. 3e), suggesting that eHsp90 internalization is an active endocytotic process reliant upon actin dynamics. Actin polymerization is involved in canonical endocytotic pathways, such as macropinocytosis and clathrin- and caveolin-mediated endocytosis, as well as the flipping of lipid rafts. A broad screen containing 140 well-characterized siRNAs against known endocytosis-related proteins was performed following HS-131 internalization (Fig. S3d and Table S1). Interestingly, none of the tested siRNAs showed a convincing effect on HS-131 internalization. The inability of pharmacological inhibitors or the siRNA screen to definitively highlight any one endocytic pathway may suggest that eHsp90 is internalized through multiple pathways.

Transformation increases Hsp90 internalization. In previous reports, expression of eHsp90 correlates with malignant phenotypes in cancer lines [14, 16, 27]. However, all cancers are derived from the transformation of non-malignant normally functioning cells. A previous report showed that overexpression of a truncated isoform of HER2 (p110HER2) that lacked the extracellular domain but was still membrane-bound led to enhanced migration, invasion, and xenograft formation of human mammary epithelial cells [28]. MCF10A cells, benign human breast epithelial cells that minimally internalize HS-131, were stably infected with a construct encoding a doxycycline-inducible p110HER2. Upon induction of p110HER2 expression, MCF10A cells exhibited a transformed phenotype as demonstrated by increased growth foci and showed a significant increase in HS-131 internalization (Figs. 3f-i). Expression of p110HER2 also increased Hsp90 expression. Whereas overexpression of a kinase-dead version of p110HER2 did increase Hsp90 expression, it did not exhibit a transformed phenotype nor did it promote internalization of HS-131 (Fig. 3f, g, i). Thus, p110HER2 may lead to a downstream signaling cascade resulting in a transformed phenotype that can be observed through HS-131 internalization. Triple negative breast tumor cells (e.g. MDA-MB-468 and 4T1) also form puncta and internalize HS-131, suggesting that eHsp90 trafficking is transformation-dependent.

eHsp90 is correlated with tumors *in vivo*. Our *in vitro* studies suggest that aggressive tumor cell lines, almost exclusively, internalize eHsp90; however, the body is comprised of hundreds of distinct cells with specific functions and in specific microenvironments. The majority of cells are fully differentiated and not actively dividing, whereas some subpopulations of cells are constantly undergoing division and growth, such as the endothelial layer lining the intestinal tract. To determine if non-tumor cells express/internalize eHsp90, we performed cryosectioning

of mice bearing MDA-MB-468 flank tumors 6 hours post HS-131 injection. Probe uptake into the tumor in the live animal was first confirmed in a Licor instrument. Cryosectioning allowed us to observe the biodistribution of fluorescent probes to the histological level throughout the body. Following sacrifice, the animal was cryopreserved and longitudinal cryosectioned in 40-μm slices. Each slice was imaged for fluorescence with an mCherry band filter (excitation 550-590 nm, emission 600-670 nm) as well as bright field (all slice image data can be down loaded at DOI:10.7924/G8G44N63). The images were reconstructed to create a 3D fluorescence and bright field images of the entire mouse anatomy (Fig. 4a and Movie S3). This process allowed for the first time a detailed examination of the complete biodistribution of HS-131 at the histological level in every organ. A control non-treated mouse was also imaged using an EGFP-mCherry dual band filter set. In a parallel study, an MS analysis was conducted on specific fluorescent tissues to confirm the presence of HS-131 parent ion (m/z = 660.0 $[M+2]^{2+}$) (Table S2).

Movie S3 shows a reconstructed flank tumor-bearing HS-131-treated mouse in 3D, first as a bright field image giving gross anatomical reference and then by HS-131 fluorescence. The 3D fluorescence movies and static images in Figs. 4a-b show bright fluorescence associated with the gall bladder, bile ducts, and upper intestinal tract in both the injected and non-injected control mouse, suggesting that it may be due to natural fluorescent compounds within the mouse food. Accordingly, MS analysis of the intestines isolated from an animal (6 hr post-drug injection) did not show the presence of the parent HS-131 ion (Table S2). In addition, the fluorescence is associated with the digested material in the lumen with no evidence of HS-131 in the gut wall or endothelial lining (Fig. 4b). Whereas diarrhea is a dose limiting toxicity associated with many

Page **11** of **26**

Hsp90 inhibitors in clinical trials and is thought to be related to inhibition of cell proliferation of the endothelial wall lining the upper and lower intestines [29], the lack of HS-131 uptake suggests that the intestinal endothelium does not internalize eHsp90. Other fluorescent regions include the Harderian glands behind the eye and the retina, the testes, and the lymph nodes (Fig. 4a and b). MS analysis of the eyes did not show evidence of the HS-131 parent ion (Table S2). Readily visible nodes include the superficial parotid node in the neck region, the proper axillary node, and the subiliac and sciatic nodes in the forelimb and hindlimb regions, respectively. Higher magnification of the individual lymph nodes shows discrete staining within the node itself confined to a few cellular structures in the hilum. Although Hsp90 inhibition has repressive effects on T lymphocytes [30], the uptake of HS-131 into the lymph nodes is unlikely to involve T cells because our studies used SCID mice. Other major organs including heart, lungs, liver, kidney, spleen, brain, skeletal muscle, stomach, skin, thyroid, prostate and fur were completely devoid of HS-131 related fluorescence at the 6 hour time point. Aside from fluorescence that had leaked from the injection site, HS-131 was cleared from the entire vasculature by the 6 hour time point. No uptake of the HS-131 was detected in the any of the skeletal structures. This was also confirmed by MS analysis (Table S2).

Significant HS-131 fluorescence was detected in the bladder and flank tumor. Overlay of the bright field image section with the fluorescence showed that all of the fluorescence was associated with urine and not the bladder itself (Fig. 4b). This was confirmed by MS analysis of the urine that detected the parent ion at a concentration approximately 50 nM (Table S2). These results suggest HS-131 is primarily eliminated intact through the kidney.

Page **12** of **26**

Examination of both the bright field image of the tumor as well as a 3D reconstruction of the tumor mass shows its anatomy including the fibrotic wall, necrotic regions, microvasculature and live tumor tissue (Fig. 4b, Movie S4). HS-131 uptake is exclusively associated with live tumor tissue and not the fibrotic wall or necrotic regions. MS analysis confirmed the presence of the intact parent HS-131 molecule at a concentration of ~325 nM (w.w.) (Table S2).

Flank tumors, due to their homogeneity, do not accurately reflect the physiology of human tumors. To investigate the tumor specificity and eHsp90 internalization in a more relevant model of human breast cancer, we turned to the MMTV-neu spontaneous mammary tumor mouse model (Figs. 4c-d). Two MMTV-neu mice bearing equal sized mammary tumors (~150 mm^3) were injected in parallel (i.v.) with 25 nmol of HS-131 or the inactive analog HS-198, and after 6 hours the animals were cryopreserved and cryosectioned as previously described. Figs. 4c and d show that the HS-131 uptake is confined to the tumor in comparison to HS-198, confirming that probe uptake is eHsp90-dependent. Importantly, HS-131 shows the same biodistribution as observed with the flank tumor animal shown in Fig. 5a. Movie S5 shows a 3D reconstruction from the HS-131-containing MMTV-neu tumor from Fig. 4d compared with that of the HS-198-treated mouse. Interestingly, compared with Movie S4, HS-131 uptake in the MMTV tumor mass is more discrete than the more homogenous uptake in the flank tumor. Closer inspection via histology revealed that HS-131 fluorescence within the MMTV tumor is confined to select areas of ductal epithelial cells (Fig. 5). Based on studies with isolated breast cell lines, these findings suggest that the cells discretely stained within HS-131 exhibit a malignant phenotype and may be analogous to ductal carcinoma *in situ* (DCIS) in human breast cancer. No uptake was observed in these cells within the tumor isolated from the HS-198-treated

Page **13** of **26**

animal, again supporting the hypothesis that HS-131 is eHsp90 dependent. In addition,

comparison with tissues from the HS-198-treated mice revealed that the previously observed

fluorescence within the rod and cone layer of the eyes and the Leydig cells of the testes were due

to autofluorescence (Fig. 5), consistent with previous reports [31].

In summary, our imaging studies with HS-131 revealed at the molecular and cellular

level that expression and internalization of eHsp90 is a unique phenomenon associated with

highly transformed tumor cells. Studies with HS-131 in other tumor cells (e.g., lung cancer and

melanoma lines) suggest that expression of eHsp90 is common to cells with an aggressive

malignant cellular phenotype (Fig. S3i). Our studies highlight the therapeutic relevance of

selectively targeting eHsp90 internalization. First eHsp90 provides a non-invasive biomarker of

malignant behavior. Second, the ability of eHsp90 to be reinternalized with a bound probe

clearly indicates the protein can be further exploited as a means of tumor-specific drug delivery.

One of the most remarkable results from our studies was the finding that expression of eHsp90 is

a rare cellular event in the body and does not occur in normal fully differentiated tissues. Given

the rareness of eHsp90 expression on cells, in principle drugs targeting eHsp90 will have

significantly greater therapeutic window than all existing Hsp90 inhibitors and offer a curative

outcome rather than conventional therapeutic approach.

METHODS

Cell culture and reagents. MDA-MB-468 cells were maintained in DMEM containing 10%

(v/v) FBS and penicillin/streptomycin. MCF10A cells were maintained in Brugge's modified

medium. Doxycycline was used at a final concentration of 1 μg/mL. Cells were kept in a

Page **14** of **26**

humidified atmosphere at 37°C and with 5% CO_2. All cells were acquired from the Duke Cancer

Institute Cell Culture Facility. PUH71 was purchased from APExBIO. All chemicals and other

reagents were of analytical grade.

HS-131 internalization assay and imaging. Cells were plated on uncoated coverslips in 12 well

plates at 150,000 cells/well and were allowed to adhere overnight. HS-131 was diluted in serum-

free/phenol red-free DMEM. After drug incubation, the cells were washed with ice-cold PBS,

fixed with 1% (w/v) PFA 10 min, and stained with 5 μg/mL wheat germ agglutinin-488 (WGA-

488, Invitrogen) and either Hoescht or DAPI. The coverslips were mounted onto microscope

slides using FluorSave (Millipore). Slides were imaged on a Leica SP5 confocal microscope.

Images were analyzed for fluorescence and puncta using ImageJ software using a non-

biased, high-throughput macro. High resolution confocal stacks were deconvolved with

Hyugen's Deconvolution Software or AiryScan.

Hsp90 colocalization. Cells were treated with HS-131 for 30 min on ice. The cells were washed

and fixed as above, blocked with 5% (v/v) normal goat serum, and incubated with anti-Hsp90

antibody (sc-7947, Santa Cruz Biotechnology, Inc.), which recognizes both the Hsp90α and

Hsp90β isoforms. The coverslips were washed and incubated with secondary antibody

conjugated to AlexaFluor-555, washed and prepared for imaging.

Biotin internalization assay. MDA-MB-468 cells were plated 1.0×10^6 cells/well in a 6-well

plate. Biotin internalization assay was performed as previously described [23]. Lysates were

collected as previously described and purified on avidin beads to collect the biotinylated

proteins. The biotinylated protein fractions were subjected to Western blot analysis.

MCF10A transformation. Human HER2 cDNAs for the full-length p185 kDa protein and its

p110 kDa fragment were cloned by PCR of cDNA from the T74D cell line. PCR-based site

specific mutation was performed to create a p110-kDa kinase inactivation by the K736R

mutation. All constructs were confirmed by sequencing. Constructs were cloned into the

doxycycline-inducible expression lentivirus plasmids using a modification of a previously

described method [32]. For the growth foci assay, cells were trypsinized, and 1,000 cells with an

inducible construct were plated with 100,000 cells uninfected MCF10A per well in a 6-well

plate. Media was replaced every 3-4 days. After 3 weeks, the cells were washed, fixed with ice

cold methanol, rinsed, and stained with a 0.4% (v/v) methylene blue solution.

Western blot analysis. Lysates were subjected to SDS-PAGE and were subsequently transferred

to a PVDF membrane. The membrane was blocked with 5% (w/v) non-fat dry milk in PBS-T

(PBS with 0.1% (v/v) Tween), incubated with anti-Hsp90, anti-HER2 (29D8, Cell Signaling

Technology) or anti-GAPDH (D16H11, Cell Signaling Technology), washed in PBS-T,

incubated with secondary antibody conjugated with HRP, and washed again in PBS-T. The

membrane was developed using Clarity Western ECL Blotting Substrate (Bio-Rad) and exposure

to film.

Three-dimensional mouse reconstruction. All protocols involving the use of mice were

approved by the Duke University IACUC. A wild-type 3-month-old male SCID mouse with a

right flank xenograft with MDA-MB-468 cells was injected with 25 nmol HS-131 through the

tail vein. Six hours later, the mouse was euthanized, prepared according to the instructions from

BioInVision, Inc. and shipped for Cryo-Imaging and reconstruction. An EGFP/mCherry dual

band filter set was used for imaging (Chroma Technology Corporation).

Histology. MMTV-neu mice treated with 10 nmol of HS-131 or HS-198 were euthanized, and

tumors, eyes, and testes were fixed in neutral-buffered formalin before dehydration and

embedding in paraffin blocks. Slices (5-µm thick) were deparaffinized and either H&E stained or

rehydrated and stained with DAPI before mounting. Slides were imaged at 20x magnification on

a Zeiss Axio Imager widefield fluorescence microscope equipped with a color camera.

Statistical analysis. All imaging experiments were performed in duplicate and repeated three

times. After testing for normalcy, multivariate analysis of variance (ANOVA) was used to detect

significant differences between experiments with more than one factor, and univariate ANOVA

was used to detect significant differences between experiments with only one factor. ANOVA

results were subjected to Bonferroni post-hoc tests to account for differences in sample size. A *p*

value of < 0.05 was considered significant. All statistical analysis was performed using IBM

SPSS Statistics for Windows, version 20.0. Data are represented as the means ± S.E.M.

ACKNOWLEDGEMENTS

Supporting Information Available: This material is available free of charge *via* the Internet. This paper contains enhanced objects.

Figures S1-S3, Table S1, Table S2, and supplementary methods.

Movies S1-S5 (Movie descriptions also available in SI).

FIGURE LEGENDS

Figure 1. HS-131 and HS-198 synthesis. (a) Structure of far-red fluorescent probes, HS-131 and HS-198. (b) Synthesis scheme of HS-131 and HS-198. (c) Simplified synthesis scheme of HS-198 precursor **14**. See also Fig. S2.

Figure 2. HS-131 is a fluorescent specific small-molecule Hsp90 inhibitor. (a) Internalization of HS-131 (25 µM, 45 min) in 67NR, 168FARN, 66cl4, 4T07, and 4T1 cells, quantified in (b); scale bar = 50 µm. (c) Dose-dependent internalization of HS-131 and HS-198 in MDA-MB-468 cells. (d) HS-131 is internalized in a time-dependent manner. (e) Fluorescence of HS-131-treated MDA-MB-468 cells (25 µM, 45 min) in competition with 1 µM HS-10 or 10 µM PUH71. (f) Biotinylated eHsp90 is detected via Western blot. B_T, total biotinylated lysate, and B_S, biotinylated lysate from stripped cells. Cells were incubated at 37°C to stimulate endocytosis, cooled, and stripped of external biotin. **, $p < 0.001$; ***, $p < 0.0001$; univariate ANOVA with Bonferroni's post-hoc test. Data are represented as the means ± SEM. See also Fig. S1.

Figure 3. HS-131 accumulates into Hsp90-positive puncta within the cell and can be induced by transformation of non-malignant cells results. (a) Three-dimensional confocal images of MDA-MB-468 cells expressing HS-131-positive puncta after a 45 min treatment with 25 µM HS-131. Scale bar, 5 µm. (b) Number of puncta/cell of MDA-MB-468 cells treated with 25 µM HS-131 at increasing time points. (c) HS-131fluorescence and Hsp90 immunoreactivity on the surface of a non-permeabilized MDA-MB-468 cell. Membrane is labeled green. Scale bar, 5 µm. (d) Number of moving puncta (tracks) detected in cells treated with 10 µM HS-131 or HS-198, or HS-131

competed with 100 µM HS-10. (e) Fluorescence of HS-131 internalization (25 µM, 45 min incubation) after treatment with endocytotic inhibitors. CytoD, cytochalasin D, 2 µM; EIPA, 5-(N-Ethyl-N-isopropyl)amiloride, 25 µM; PitStop2, 25 µM; Filipin III, 5.0 µg/mL. (f) Representative Western blot of MCF10A clones showing HER2 and Hsp90 expression. GAPDH was used as an internal loading control. (g) Growth foci in MCF10A cells overexpressing full-length HER2, p110HER2, or p110HER2KD induced with doxycycline. (h) Representative fluorescence images of MCF10A mutants treated with 25 µM HS-131 for 45 min. Scale bar, 50 µm. (i) Quantification of HS-131 fluorescence taken as a ratio of doxycycline-treated cells to non-induced cells. *, $p < 0.05$; **, $p < 0.001$, univariate ANOVA with Bonferroni's post-hoc test. Data are represented as the means ± SEM. See also Fig. S3.

Figure 4. HS-131 can be visualized in tumors *in vivo*. (a) Left: Mouse with right flank xenograft tumor formed from MDA-MB-468 cells. Right: control mouse (no tumor or drug treatment). Arrowhead, tumor; 1, injection site; 2, bladder; 3, gallbladder; 4, lymph nodes; 5, testes; 6, Harderian glands. (b) Fluorescence and brightfield images in representative 40-µm section of tumor and other organs; LN, lymph node. (c) Top: HS-131-treated MMTV-neu mouse with spontaneous tuor near left rear leg. Bottom: HS-198-treated MMTV-neu mouse with spontaneous tumor on bottom right abdomen. Arrowheads indicate tumor location. (d) Cross-section of tumor with drug fluorescence. See also Movies S3-S5.

Figure 5. Histology of fluorescent tissues reveals tumor specificity. Serial sections of various organs were imaged, either with H&E staining or with DAPI/Cy5 (drug) fluorescence. Specific drug fluorescence is observed in duct epithelium of tumor cells in the HS-131-treated mouse, but

not in the HS-198-treated mouse. Tissues from the HS-198-treated mouse reveal

autofluorescence in the rods and cones layer of the eye and in the Leydig cells of the testes.

References

[1] Moulick, K., Ahn, J. H., Zong, H., Rodina, A., Cerchietti, L., Gomes DaGama, E. M.,

    Caldas-Lopes, E., Beebe, K., Perna, F., Hatzi, K., Vu, L. P., Zhao, X., Zatorska, D.,

    Taldone, T., Smith-Jones, P., Alpaugh, M., Gross, S. S., Pillarsetty, N., Ku, T., Lewis, J.

    S., Larson, S. M., Levine, R., Erdjument-Bromage, H., Guzman, M. L., Nimer, S. D.,

    Melnick, A., Neckers, L., and Chiosis, G. (2011) Affinity-based proteomics reveal

    cancer-specific networks coordinated by Hsp90, *Nat. Chem. Biol. 7*, 818-826.

[2] Taipale, M., Jarosz, D. F., and Lindquist, S. (2010) HSP90 at the hub of protein homeostasis:

    emerging mechanistic insights, *Nat. Rev. Mol. Cell Biol. 11*, 515-528.

[3] Whitesell, L., and Lindquist, S. L. (2005) HSP90 and the chaperoning of cancer, *Nat. Rev.*

    Cancer 5, 761-772.

[4] Neckers, L., and Workman, P. (2012) Hsp90 molecular chaperone inhibitors: are we there

    yet?, *Clin. Cancer. Res. 18*, 64-76.

[5] Pearl, L. H., and Prodromou, C. (2006) Structure and mechanism of the Hsp90 molecular

    chaperone machinery, *Annu. Rev. Biochem. 75*, 271-294.

[6] Trepel, J., Mollapour, M., Giaccone, G., and Neckers, L. (2010) Targeting the dynamic

    HSP90 complex in cancer, *Nat. Rev. Cancer 10*, 537-549.

[7] Jhaveri, K., Taldone, T., Modi, S., and Chiosis, G. (2012) Advances in the clinical development of heat shock protein 90 (Hsp90) inhibitors in cancers, *Biochim. Biophys. Acta 1823*, 742-755.

[8] Pillarsetty, N. C.-L., E.; Punzalan, B.; Santos, E.; Kang, Y.; Taldone, T.; Zatorska, D.; Chiosis, G.; Lewis, J.; Larson, S. (2010) Radioiodination, biodistribution, and PET imaging studies of Hsp90 inhibitor [^{124}I]-PU-H71 (Abstract No. 556), In *Society of Nuclear Medicine and Molecular Imaging*, p 556, Salt Lake City, Utah, USA.

[9] Taldone, T., Zatorska, D., Ochiana, S. O., Smith-Jones, P., Koziorowski, J., Dunphy, M. P., Zanzonico, P., Bolaender, A., Lewis, J. S., Larson, S. M., Chiosis, G., and Pillarsetty, N. V. (2016) Radiosynthesis of the iodine-124 labeled Hsp90 inhibitor PU-H71, *J Labelled Comp Radiopharm 59*, 129-132.

[10] Kamal, A., Thao, L., Sensintaffar, J., Zhang, L., Boehm, M. F., Fritz, L. C., and Burrows, F. J. (2003) A high-affinity conformation of Hsp90 confers tumour selectivity on Hsp90 inhibitors, *Nature 425*, 407-410.

[11] Woodford, M. R., Truman, A. W., Dunn, D. M., Jensen, S. M., Cotran, R., Bullard, R., Abouelleil, M., Beebe, K., Wolfgeher, D., Wierzbicki, S., Post, D. E., Caza, T., Tsutsumi, S., Panaretou, B., Kron, S. J., Trepel, J. B., Landas, S., Prodromou, C., Shapiro, O., Stetler-Stevenson, W. G., Bourboulia, D., Neckers, L., Bratslavsky, G., and Mollapour, M. (2016) Mps1 Mediated Phosphorylation of Hsp90 Confers Renal Cell Carcinoma Sensitivity and Selectivity to Hsp90 Inhibitors, *Cell Rep 14*, 872-884.

[12] Murshid, A., Gong, J., and Calderwood, S. K. (2014) Hsp90-peptide complexes stimulate antigen presentation through the class II pathway after binding scavenger receptor SREC-I, *Immunobiology 219*, 924-931.

[13] McCready, J., Wong, D. S., Burlison, J. A., Ying, W., and Jay, D. G. (2014) An Impermeant Ganetespib Analog Inhibits Extracellular Hsp90-Mediated Cancer Cell Migration that Involves Lysyl Oxidase 2-like Protein, *Cancers (Basel) 6*, 1031-1046.

[14] Becker, B., Multhoff, G., Farkas, B., Wild, P. J., Landthaler, M., Stolz, W., and Vogt, T. (2004) Induction of Hsp90 protein expression in malignant melanomas and melanoma metastases, *Exp Dermatol 13*, 27-32.

[15] Sidera, K., and Patsavoudi, E. (2008) Extracellular HSP90: conquering the cell surface, *Cell Cycle 7*, 1564-1568.

[16] Barrott, J. J., Hughes, P. F., Osada, T., Yang, X. Y., Hartman, Z. C., Loiselle, D. R., Spector, N. L., Neckers, L., Rajaram, N., Hu, F., Ramanujam, N., Vaidyanathan, G., Zalutsky, M. R., Lyerly, H. K., and Haystead, T. A. (2013) Optical and radioiodinated tethered Hsp90 inhibitors reveal selective internalization of ectopic Hsp90 in malignant breast tumor cells, *Chem. Biol. 20*, 1187-1197.

[17] Imai, T., Kato, Y., Kajiwara, C., Mizukami, S., Ishige, I., Ichiyanagi, T., Hikida, M., Wang, J. Y., and Udono, H. (2011) Heat shock protein 90 (HSP90) contributes to cytosolic translocation of extracellular antigen for cross-presentation by dendritic cells, *Proc Natl Acad Sci U S A 108*, 16363-16368.

[18] Fadden, P., Huang, K. H., Veal, J. M., Steed, P. M., Barabasz, A. F., Foley, B., Hu, M., Partridge, J. M., Rice, J., Scott, A., Dubois, L. G., Freed, T. A., Silinski, M. A., Barta, T.

Page **23** of **26**

E., Hughes, P. F., Ommen, A., Ma, W., Smith, E. D., Spangenberg, A. W., Eaves, J.,

Hanson, G. J., Hinkley, L., Jenks, M., Lewis, M., Otto, J., Pronk, G. J., Verleysen, K.,

Haystead, T. A., and Hall, S. E. (2010) Application of chemoproteomics to drug

discovery: identification of a clinical candidate targeting hsp90, *Chem. Biol. 17*, 686-694.

[19] Hughes, P. F., Barrott, J. J., Carlson, D. A., Loiselle, D. R., Speer, B. L., Bodoor, K., Rund,

L. A., and Haystead, T. A. (2012) A highly selective Hsp90 affinity chromatography

resin with a cleavable linker, *Bioorg. Med. Chem. 20*, 3298-3305.

[20] Lee, H., Mason, J. C., and Achilefu, S. (2006) Heptamethine cyanine dyes with a robust C-

C bond at the central position of the chromophore, *J Org Chem 71*, 7862-7865.

[21] Wycisk, V., Pauli, J., Welker, P., Justies, A., Resch-Genger, U., Haag, R., and Licha, K.

(2015) Glycerol-based contrast agents: a novel series of dendronized pentamethine dyes,

Bioconjug Chem 26, 773-781.

[22] Lu, X., Bennet, B., Mu, E., Rabinowitz, J., and Kang, Y. (2010) Metabolomic changes

accompanying transformation and acquisition of metastatic potential in a syngeneic

mouse mammary tumor model, *J. Biol. Chem. 285*, 9317-9321.

[23] Gabriel, L., Stevens, Z., and Melikian, H. (2009) Measuring plasma membrane protein

endocytic rates by reversible biotinylation, *J Vis Exp*.

[24] Prodromou, C., Roe, S. M., O'Brien, R., Ladbury, J. E., Piper, P. W., and Pearl, L. H. (1997)

Identification and structural characterization of the ATP/ADP-binding site in the Hsp90

molecular chaperone, *Cell 90*, 65-75.

[25] Obermann, W. M., Sondermann, H., Russo, A. A., Pavletich, N. P., and Hartl, F. U. (1998) In vivo function of Hsp90 is dependent on ATP binding and ATP hydrolysis, *J. Cell Biol. 143*, 901-910.

[26] Scheibel, T., Neuhofen, S., Weikl, T., Mayr, C., Reinstein, J., Vogel, P. D., and Buchner, J. (1997) ATP-binding properties of human Hsp90, *J. Biol. Chem. 272*, 18608-18613.

[27] Eustace, B. K., Sakurai, T., Stewart, J. K., Yimlamai, D., Unger, C., Zehetmeier, C., Lain, B., Torella, C., Henning, S. W., Beste, G., Scroggins, B. T., Neckers, L., Ilag, L. L., and Jay, D. G. (2004) Functional proteomic screens reveal an essential extracellular role for hsp90 alpha in cancer cell invasiveness, *Nat. Cell Biol. 6*, 507-514.

[28] Ward, T. M., Iorns, E., Liu, X., Hoe, N., Kim, P., Singh, S., Dean, S., Jegg, A. M., Gallas, M., Rodriguez, C., Lippman, M., Landgraf, R., and Pegram, M. D. (2013) Truncated p110 ERBB2 induces mammary epithelial cell migration, invasion and orthotopic xenograft formation, and is associated with loss of phosphorylated STAT5, *Oncogene 32*, 2463-2474.

[29] Goldman, J. W., Raju, R. N., Gordon, G. A., El-Hariry, I., Teofilivici, F., Vukovic, V. M., Bradley, R., Karol, M. D., Chen, Y., Guo, W., Inoue, T., and Rosen, L. S. (2013) A first in human, safety, pharmacokinetics, and clinical activity phase I study of once weekly administration of the Hsp90 inhibitor ganetespib (STA-9090) in patients with solid malignancies, *BMC Cancer 13*, 152.

[30] Bae, J., Munshi, A., Li, C., Samur, M., Prabhala, R., Mitsiades, C., Anderson, K. C., and Munshi, N. C. (2013) Heat shock protein 90 is critical for regulation of phenotype and functional activity of human T lymphocytes and NK cells, *J. Immunol. 190*, 1360-1371.

[31] Yang, Y., and Honaramooz, A. (2012) Characterization and quenching of autofluorescence

in piglet testis tissue and cells, *Anat Res Int 2012*, 820120.

[32] Shin, K. J., Wall, E. A., Zavzavadjian, J. R., Santat, L. A., Liu, J., Hwang, J. I., Rebres, R.,

Roach, T., Seaman, W., Simon, M. I., and Fraser, I. D. (2006) A single lentiviral vector

platform for microRNA-based conditional RNA interference and coordinated transgene

expression, *Proc Natl Acad Sci U S A 103*, 13759-13764.
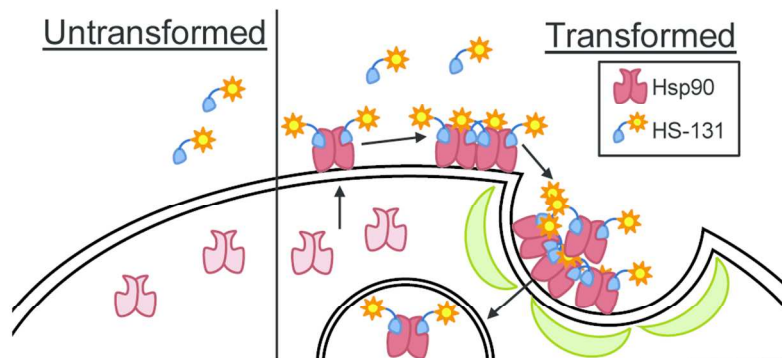
Graphical ToC

112x79mm (300 x 300 DPI)
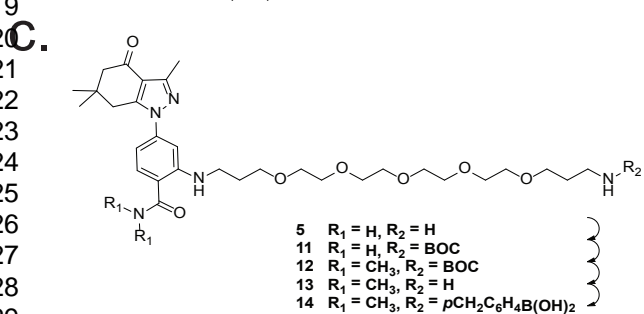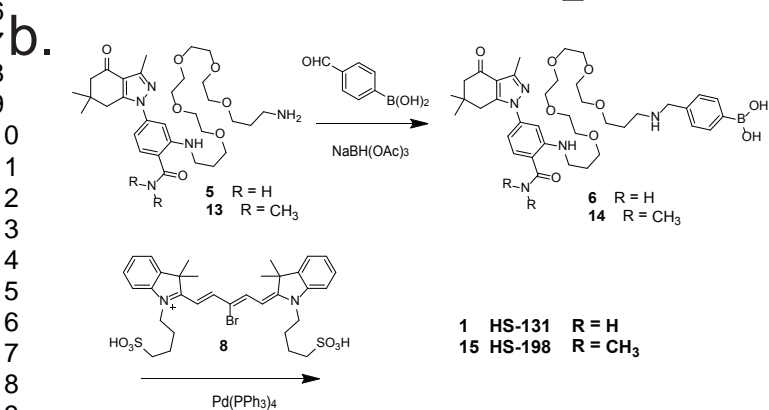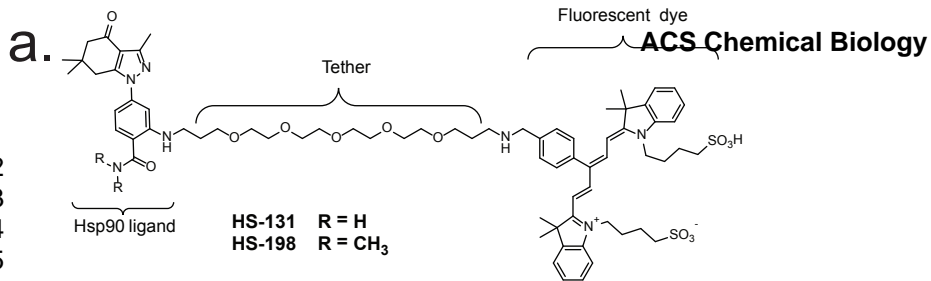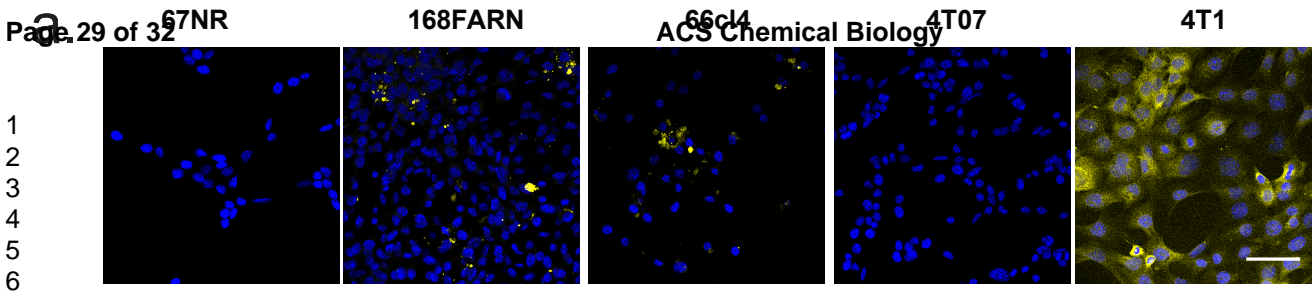
a.

Fluorescent dye

Tether

Hsp90 ligand

HS-131 **R = H**
HS-198 **R = CH₃**

b.

OHC— B(OH)₂

NaBH(OAc)₃

5   R = H
13 R = CH₃

6   R = H
14 R = CH₃

8

Pd(PPh₃)₄

1   **HS-131** **R = H**
15 **HS-198** **R = CH₃**

c.

5   R₁ = H, R₂ = H
11 R₁ = H, R₂ = BOC
12 R₁ = CH₃, R₂ = BOC
13 R₁ = CH₃, R₂ = H
14 R₁ = CH₃, R₂ = *p*CH₂C₆H₄B(OH)₂

1
2
3
4
5
6
7
8
9
10
11
12
13
14
15
16
17
18
19
20
21
22
23
24
25
26
27
28
29
30
31
32
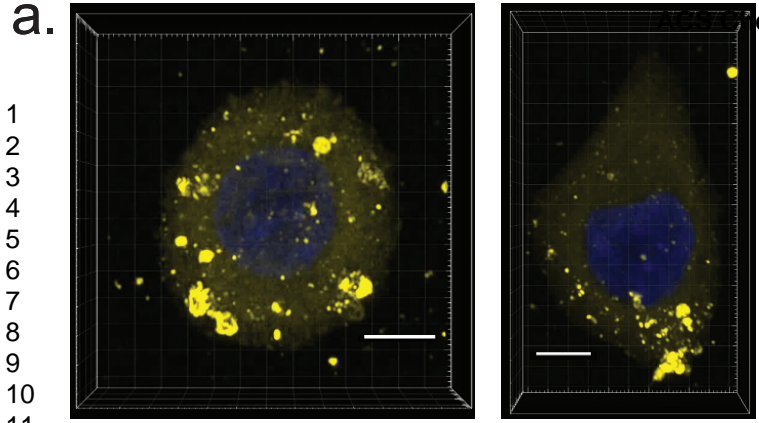33
34
35
36
37
38
39
40
41
42
43
44
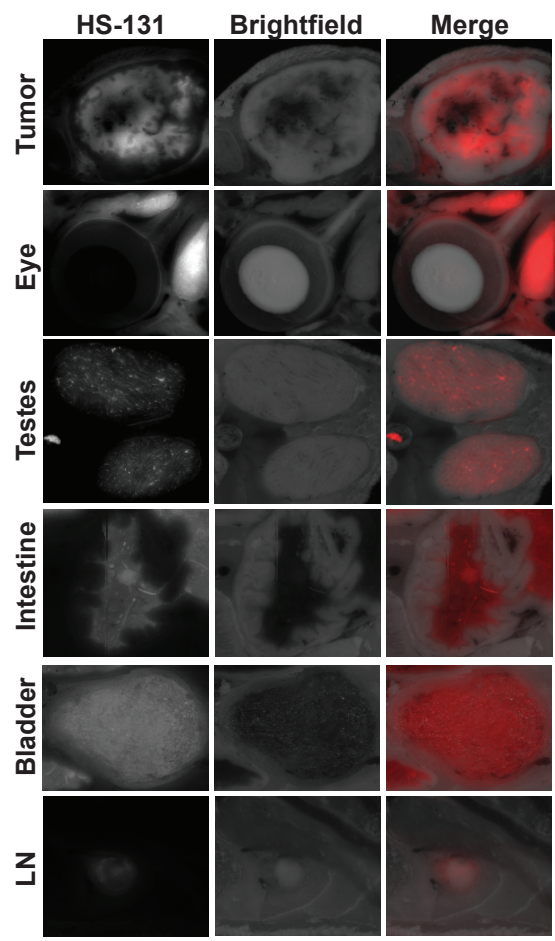45
46
47
48
49
50
51
52
53
54
55
56
57
58
59
60

1
2
3
4
5
6
7
8
9
10
11
12
13
14
15
16
17
18
19
20
21
22
23
24
25
26
27
28
29
30
31
32
33
34
35
36
37
38
39
40
41
42
43
44
45
46
47
48
49
50
51
52
53
54
55
56
57
58
59
60
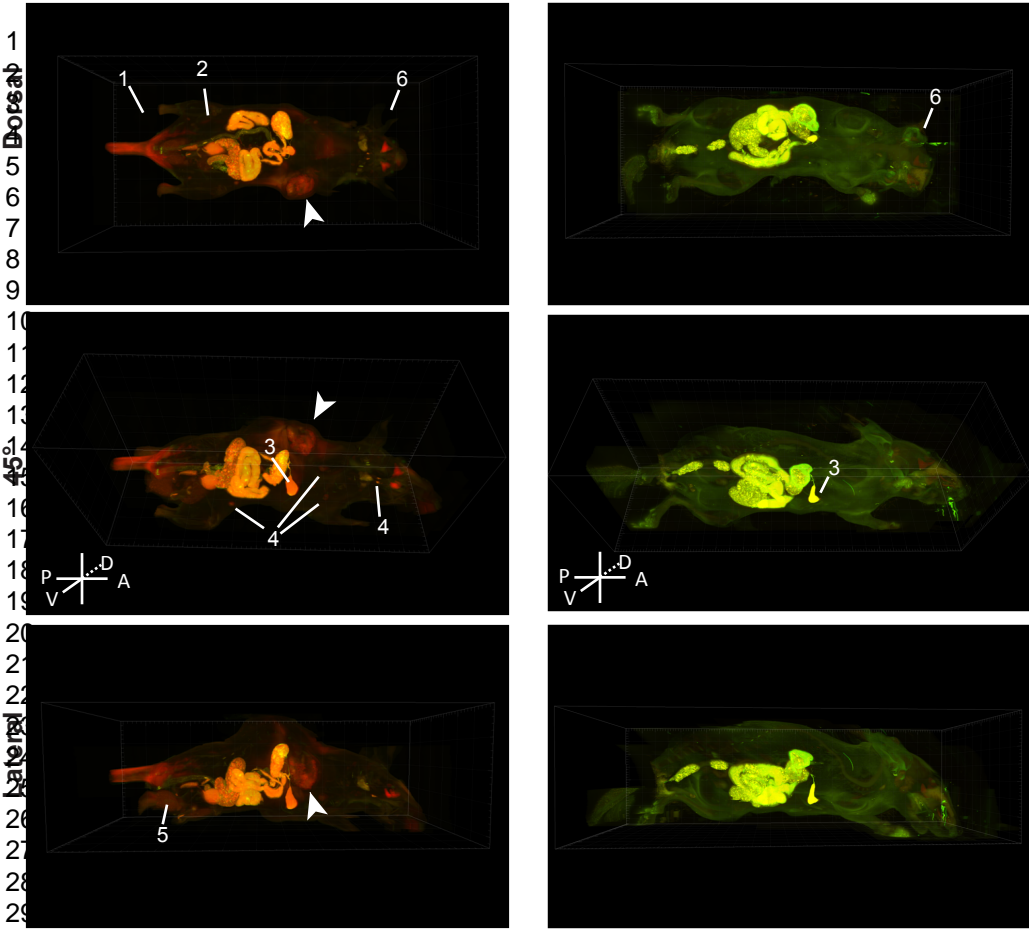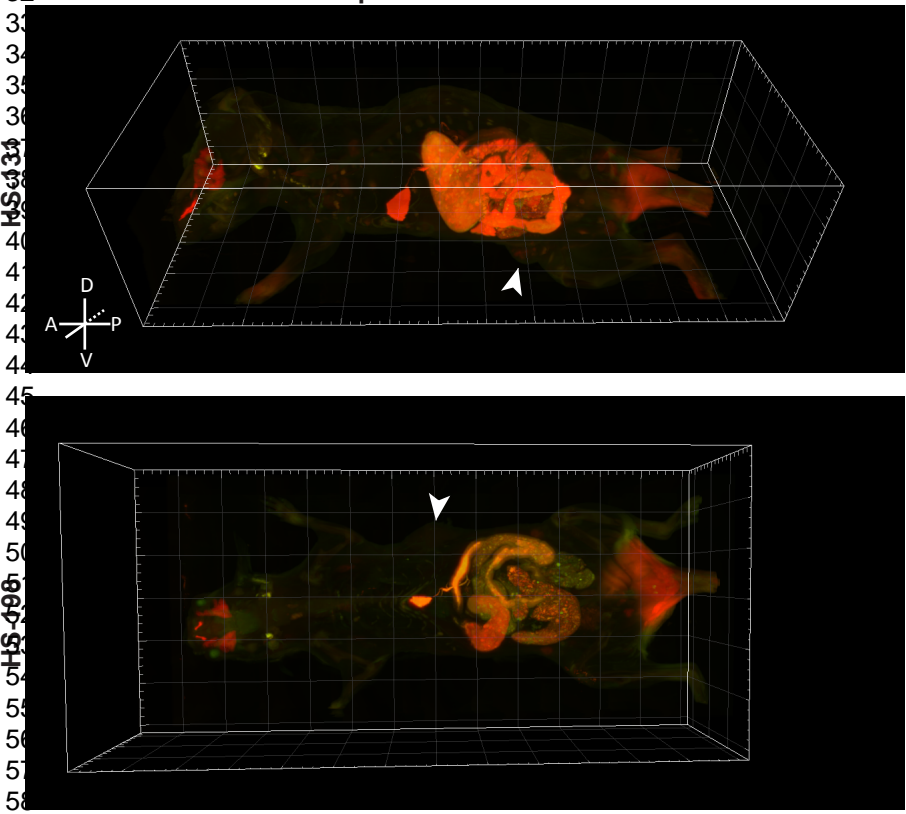
a.

MDAMB468 Flank Tumor
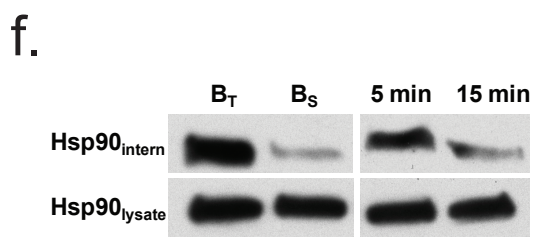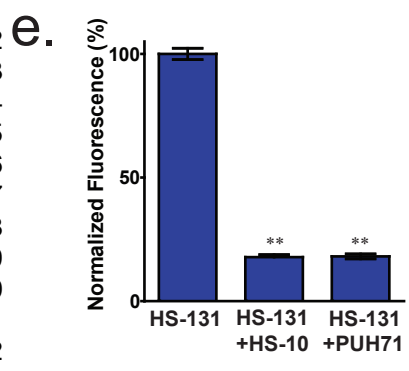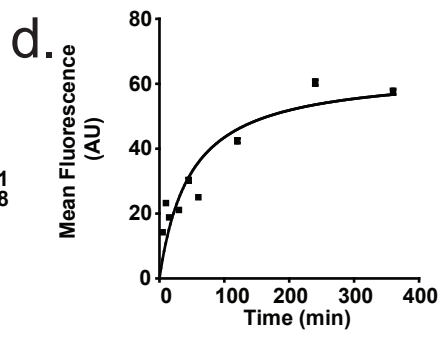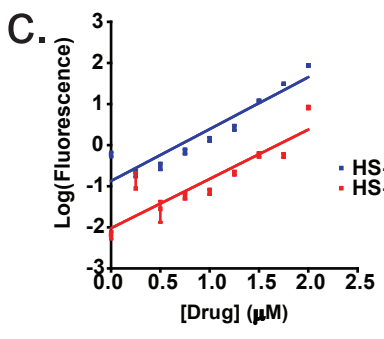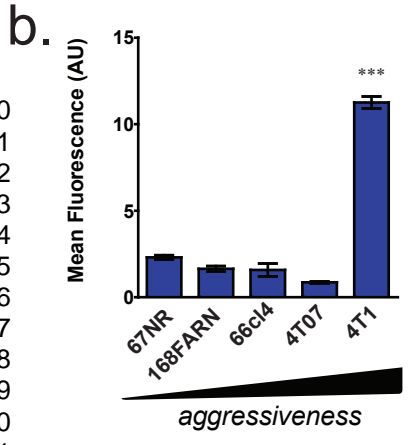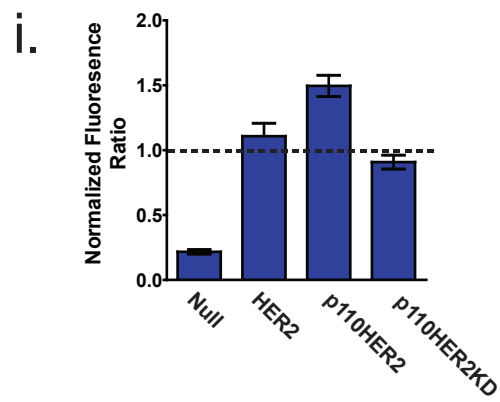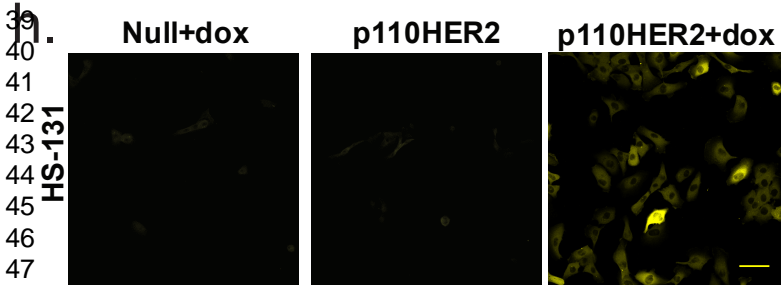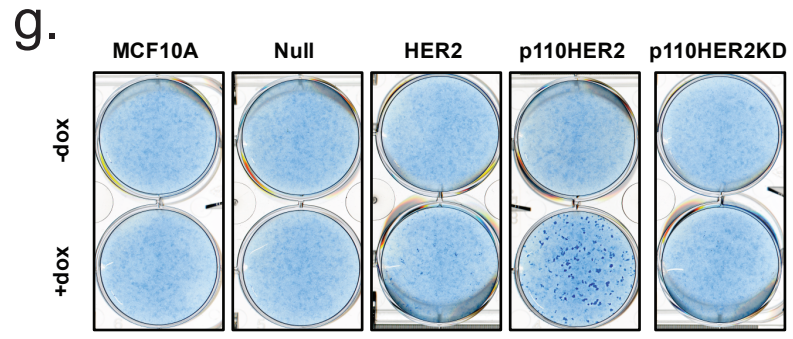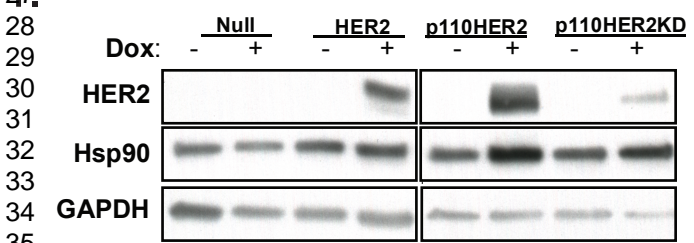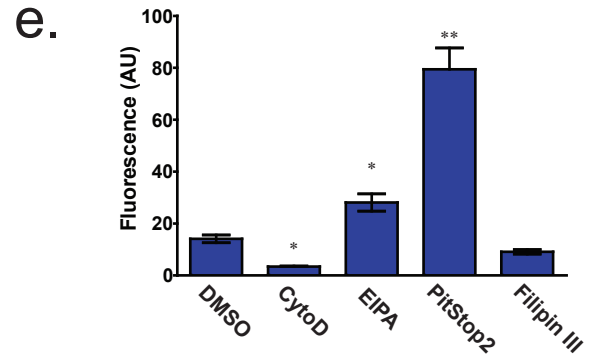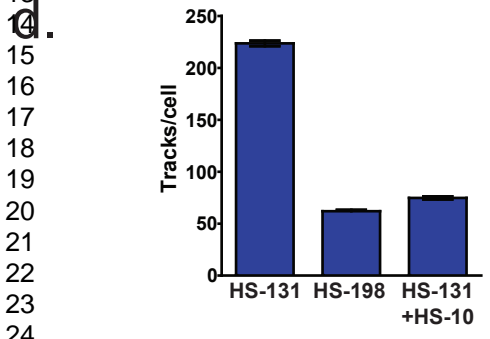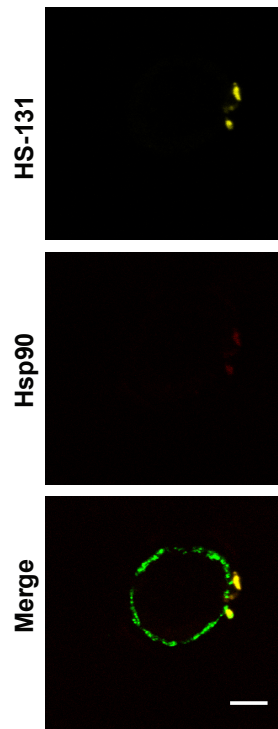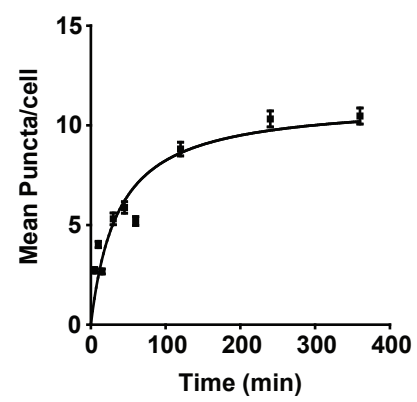
HS-131-injected mouse | Non-injected mouse

b.

	HS-131	Brightfield	Merge
Tumor			
Eye			
Testes			
Intestine			
Bladder			
LN			

c.

MMTV-Neu Spontaneous Tumor Model

d.

	Drug	Brightfield	Merge
HS-131			
HS-198			